Research Article

Received: 27 April 2020 Revised: 17 June 2020 Accepted article published: 10 July 2020 Published online in Wiley Online Library:

(wileyonlinelibrary.com) DOI 10.1002/pi.6083

Polylactide-perylene derivative for blue biodegradable organic light-emitting diodes

Hameed Al-Attar,[a,b] Aula A Alwattar,[c,d*] Athir Haddad,[c,d] Bassil A Abdullah,[a] Peter Quayle[d] and Stephen G Yeates[d]

Abstract

In this work we demonstrate, for the first time, the use of polylactic acid (PLA) as a biodegradable host matrix for the construction of the active emissive layer of organic light-emitting diode (OLED) devices for potential use in bioelectronics. In this preliminary study, we report a robust synthesis of two fluorescent PLA derivatives, pyrene-PLA (AH10) and perylene-PLA (AH11). These materials were prepared by the ring opening polymerisation of L-lactide with hydroxyalkyl-pyrene and hydroxyalkyl-perylene derivatives using 1,8-diazabicyclo[5.4.0]undec-7-ene as catalyst. OLEDs were fabricated from these materials using a simple device architecture involving a solution-processed single-emitting layer in the configuration ITO/PEDOT:PSS/PVK:OXD-7 (35%):AH10 or AH11 (20%)/TPBi/LiF/Al (ITO, indium tin oxide; PEDOT:PSS, poly(3,4-ethylenedioxythiophene) doped with poly (styrenesulfonic acid); PVK, poly(vinylcarbazole); OXD-7, (1,3-phenylene)-bis-[5-(4-tert-butylphenyl)-1,3,4-oxadiazole]; TPBi, 2,2′,2″-(1,3,5-benzenetriyl)tris(1-phenyl-1H-benzimidazole)). The turn-on voltage for the perylene OLED at 10 cd m^{-2} was around 6 V with a maximum brightness of 1200 cd m^{-2} at 13 V. The corresponding external quantum efficiency and device current efficiency were 1.5% and 2.8 cd A^{-1} respectively. In summary, this study provides proof of principle that OLEDs can be constructed from PLA, a readily available and renewable bio-source.

Supporting information may be found in the online version of this article.

Keywords: bioelectronics; biodegradable; organic light-emitting diode; polylactic acid; perylene

INTRODUCTION

Organic electronics are ideally suited for the interface with biology. The 'soft' nature of organic materials offers better mechanical compatibility with tissue compared to traditional electronic materials, while their compatibility with mechanically flexible substrates is eminently suited for their fabrication into biomedical implants.[1,2] More importantly, their ability to conduct ions in addition to electrons and holes opens up a new communication channel with biology. A key aspect to this is the ability to be able to use biodegradable and biocompatible materials wherever possible.[3,4]

A number of synthetic (e.g. polylactic acid (PLA),[5] polycaprolactone,[6] polyvinyl alcohol[7,8]) and naturally occurring polymers (derived from paper,[9–12] silk,[13,14] gelatin,[15–17] cellulose-based polymers[18–20]), all of which are derived from renewable resources, have found application as either substrate or dielectric material in the fabrication of electronic devices. Future developments, especially in the area of personalised electronic devices, will require the fabrication of electronic implants which are capable of undergoing controlled degradation within the human body.[21,22]

PLA has a number of biomedical applications, especially in drug delivery, due to its optical transparency, biocompatibility, non-toxicity and tunable chemical stability.[22–25] In addition PLA, with a volume resistivity of the order of 10^9 Ω cm, is a high frequency insulator[26,27] and has been widely used in the fabrication of flexible sensors where the permanent dipole associated with the ester carbonyl moiety enables charge trapping which results in enhanced photosensitivity and thermal sensitivity.[28] Key to our work is the seminal contribution by Wu *et al.*[29] in which PLA was utilised to construct an organic semiconductor/dielectric interface in the fabrication of organic transistors. Mattana *et al.*[5] have also utilised PLA in the fabrication of biodegradable organic field-effect transistors and organic electrochemical transistors. Zimmermann *et al.*[30] recently employed poly(lactic-*co*-glycolic acid) (PLGA) as an ion-conducting polymer for biodegradable light-emitting electrochemical cells, where PLGA was used to promote ionic conductivity in the active layer of the light-emitting electrochemical cells. These studies highlight the possibility of fabricating low-cost organic electronic devices starting from renewable

* *Correspondence to: AA Alwattar, Departmment of Chemistry, University of Manchester, Manchester M13 9PL, UK; Department of Chemistry, College of Science, University of Basrah, Garmat Ali, 61004, Basrah, Iraq. E-mail: aula.alwattar@manchester.ac.uk; ula.jumah@uobasrah.edu.iq*

a *Department of Physics, College of Science, University of Basrah, Basrah, Iraq*

b *Department of Physics, University of Durham, Durham, UK*

c *Department of Chemistry, College of Science, University of Basrah, Basrah, Iraq*

d *Departmment of Chemistry, University of Manchester, Manchester, UK*

feedstocks which have a negligible end of life footprint.[31] Critical to biomedical applications is the observation that PLA, and related co-polymers, are found to undergo controlled hydrolysis under physiological conditions (37 °C, pH 7.4) leading to the generation of benign by-products.[32] Germaine to our investigation is the recent report from Rogers and colleagues[32,33] concerning the development of 'transient', biodegradable light-emitting diodes (LEDs) based upon ZnO. The use of PLA as an organic support[34,32] in the construction of biodegradable LEDs has not been reported previously, to our knowledge, and is a development which we now wish to disclose in this paper.[35,36]

Pyrene and perylene are highly emissive chromophores, their light emission being in the deep blue–UV (377–420 nm) and blue (450 nm) regions of the electromagnetic spectrum respectively. Both pyrene and perylene are planar, polycyclic aromatic hydrocarbons which demonstrate a tendency for self-aggregation in both the solid and solution state. Co-facial aggregation in this manner (generating structures which are stabilised by π–π interactions) results in substantial red shifts in fluorescence emission spectra and a decrease in fluorescence quantum yields (Φ_f). However, in dilute solutions, where π stacking is minimised, optical quantum yields (Φ_f) for both of these compounds can exceed 90%.[37] We reasoned that incorporation of a pyrene or perylene moiety into a PLA matrix would prevent π–π stacking and that these fluorophores would therefore behave as in dilute solution and exhibit their usual emissive properties.[38,39]

In a novel departure we report the fabrication and evaluation of an organic LED (OLED) device using solution processing techniques[40–43] which utilises PLA as the supporting matrix. In this study we find that the incorporation of perylene residues (**AH11**) as fluorophore within the PLA matrix generates material suitable for OLED fabrication. We note the potential generality of this approach by the synthesis of a pyrene-based fluorophore (**AH10**)[44] whose incorporation into OLED devices is currently under investigation. Both **AH10** and **AH11** were readily available from the ring opening polymerisation of L-lactide (L-LA) with hydroxyalkyl-pyrene and hydroxyalkyl-perylene derivatives using 1,8-diazabicyclo[5.4.0]undec-7-ene (DBU) as catalyst. The choice of alcohol partner, in this proof of principle investigation, was dictated by their ease of preparation from the requisite bromoaromatic using well established, palladium-catalysed, cross-coupling methodologies. This approach provides great flexibility and, in principle, enables the incorporation of a broad range of fluorophores into the PLA matrix. Since PLA derivatives have high resistivity, additional electron and hole transport materials are required to improve device conductivity and to achieve charge balance.

In this study poly(vinylcarbazole) (PVK) and (1,3-phenylene)-bis-[5-(4-tert-butylphenyl)-1,3,4-oxadiazole] (OXD-7) were used as hole and electron transport materials, respectively. PLA behaves as an electrical insulator, a property which has been put to full effect in the fabrication of plastic electronic devices. We wish to emphasise that in this work we demonstrate, to the best of our knowledge for the first time, the use of PLA as a biodegradable host matrix for the construction of the active emissive layer of OLED devices.

EXPERIMENTAL

Materials

All reactants, reagents and dry solvents were purchased from Merck, Arcos Organics and Fisher Scientific and were used without further purification. Column chromatography was performed using Davisil grade 636 (60 Å pore size, 40–63 mesh) silica gel. Thin-layer chromatography (TLC) was carried out using DC-Fertigfolie POLYGRAM® SIL G/UV254 percolated TLC sheets with substrate detection by UV light (254 and 365 nm).

Material characterisation

Matrix-assisted laser desorption/ionisation (MALDI) mass spectra were acquired with a Shimadzu Axima Confidence instrument using a trans-2-[3-(4-*tert*-butylphenyl)-2-methyl-2-propenylidene]malononitrile (DCTB) and dithranol. High-resolution mass spectra were obtained using a Thermo Exactive Plus EMR or Thermo Finnigan MAT95XP mass spectrometer. ^{1}H NMR (500 MHz) spectra were recorded using a Bruker Avance II+ spectrometer referencing to the residual protons in $CDCl_3$ (7.27 ppm). ^{13}C NMR spectra (126 MHz) were recorded using a Bruker Avance II+ spectrometer referencing to the residual solvent peak as appropriate: $CDCl_3$ (77.00 ppm). All coupling constants (J) are reported in hertz and chemical shifts (λ) are reported in parts per million. Signal multiplicities are designated as singlet (s), doublet (d), triplet (t), quartet (q), multiplet (m) or any collection of these. IR spectra were recorded using a Thermo Scientific Nicolet iS5 spectrometer with an iDS ATR accessory in the solid state. UV–visible spectra were recorded using a Varian Eclipse 5000 spectrophotometer between 200 nm and 800 nm using quartz cuvettes with a path length of 1 cm. Fluorescence spectra were recorded on a Varian Eclipse fluorescence spectrometer. Samples were irradiated (λ_{ex} = 320 nm) in quartz cuvettes (10 mm) and emission spectra (λ_{em}) were recorded between 300 nm and 600 nm. Gel permeation chromatography (GPC) was used to determine the molecular weight of polymers in tetrahydrofuran with a flow rate of 1 mL min^{-1} (1–2 mg mL^{-1}) at 40 °C using a Viscotek GPCmax VE2001 solvent/sample module with a 2 × PL gel 10 µm MIXED-B and a 1 × PL gel 500A column and a Viscotek VE3580 refractive index detector. The system was calibrated with low-polydispersity polystyrene standards, in the range 200 to 6 × 10^6 g mol^{-1}. DSC measurements were obtained with a PerkinElmer Diamond DSC under nitrogen at a heating rate of 10 °C min^{-1}.

Synthesis and characterisation of PLA derivatives

Synthesis of 5-(perylen-3-yl)pent-4-yn-1-ol

5-(Perylen-3-yl)pent-4-yn-1-ol was prepared by a modified literature synthesis.[37,45]

To a two-neck round bottom flask (250 mL) was added 3-bromoperylene[46] (1.4 g, 4.22 mmol), $Pd(PPh_3)_4$ (273 mg, 0.24 mmol, 6 mol%) and CuI (37.9 mg, 0.39 mmol, 9 mol%) and the flask was then purged with N_2. In a separate two-neck round bottom flask (100 mL) was added, via syringe, dry tetrahydrofuran (49 mL) and Et_3N (35 mL) and the solution was sparged with N_2 for 25 min prior to the addition of 4-pentyn-1-ol (1 mL, 10.5 mmol). This solution was transferred, via syringe, to the first reaction vessel, which was then heated at 70 °C for 2 h. On cooling to ambient temperature the reaction mixture was concentrated *in vacuo* and the residue purified by column chromatography ('dry-loaded'; silica; gradient elution with CH_2Cl_2-petroleum ether 3:7 v/v to ethyl acetate-petroleum ether 3:2 v/v), to afford the title compound (930 mg, 66% yield) as a yellow-orange solid, melting point 188–190 °C.

^{1}H NMR: δ (500 MHz, $CDCl_3$) δ 1.52 (1 H br, s, O–H), 2.00 (2 H, quin, J = 6.8 Hz, 2 H, C–C–H), 2.7 (2 H, t, J = 6.8 Hz, C≡C–C–H), 3.93 (2 H, t, J = 6.8 Hz, O–C–H), 7.50 (2 H, td, J = 7.8, 3.0 Hz, Ar–H), 7.57 (1 H, t, J = 7.9 Hz, Ar–H), 7.62 (1 H, d, J = 7.9 Hz, C(2)H),

7.70 (2 H, d, $J = 8.1$ Hz, Ar–H), 8.12 (1 H, d, $J = 7.9$ Hz, C(1)H), 8.17–8.26 (4 H, m, Ar–H) ppm. ^{13}C NMR: (126 MHz, $CDCl_3$) δ 16.7, 31.9, 62.2, 79.6, 95.5, 119.6, 120.5, 120.6, 120.7, 120.9, 126.1, 126.5, 126.6, 128.0, 128.1, 128.4, 128.5, 130.8, 131.1, 131.2, 131.4, 131.8, 131.4, 134.6, 134.8 ppm. IR: $\bar{\nu}_{max}$/cm^{-1} 3280 O–H (br), 3049.9 and 2942 (Ar C–H), 2880 (C–H), 2217.7 (C≡C), 1600 and 1588 (Ar C=C) and 1188 (C–O). MS: (*m/z*, MALDI-dithranol) 334.6 ([M]$^+$, 100%), 335.6 ([M + H]$^+$, 28%), 226.4 ([dithranol]$^+$, 30%), 225.3 (45). High resolution mass spectrometry (ESI$^+$) $C_{25}H_{19}O$ ([M + H]$^+$) requires 335.1430, found 335.1425. These data are in accord with those reported in the literature for this compound.[37,45]

*Preparation of pyrene-PLA (**AH10**) and perylene-PLA (**AH11**)*

AH10 was synthesised using our previously reported procedure and the ^{1}H NMR and ^{13}C NMR spectra are shown in Fig. S1 in Appendix S1.[44] **AH11** was synthesised using this same procedure as described below.

To a solution of 5-(perylen-3-yl)pent-4-yn-1-ol (334 mg, 1 mmol) and L-LA (1.3 g, 3 mmol) in dry CH_2Cl_2 (15 mL) was added DBU (20 µL, 1% of the total monomer weight) and the resultant reaction mixture was stirred for 24 h at 25 °C under an atmosphere of nitrogen. The crude product was purified using column chromatography (silica gel; eluent 100% CH_2Cl_2 and then 100% MeOH). The solution was concentrated *in vacuo* at 25 °C and precipitation of the polymer was achieved by the dropwise addition of this solution to 500 mL of diethyl ether which was then collected by vacuum filtration. The precipitated polymer was washed with diethyl ether (5 × 20 mL) and dried under vacuum (1 Torr) at 25 °C for 24 h to obtain the purified polymer as a bright yellow solid. The ^{1}H NMR and ^{13}C NMR spectra for **AH11** are shown in Fig. 1.

Device preparation

Devices were fabricated on indium tin oxide (ITO) coated glass substrates of thickness 125 nm and possessing a sheet resistance of 15 Ω cm. Poly(3,4-ethylenedioxythiophene) doped with a high work function hole-injecting layer poly(styrenesulfonic acid) (PEDOT:PSS) was spin-coated at 4000 rpm for 60 s to produce a *ca* 35 nm thick hole-injecting layer. The PEDOT:PSS layer was annealed at *ca* 200 °C for 5 min to remove any residual water. A solution of 12 mg mL^{-1} PVK (M_w = 90 000) mixed with 40% w/w of OXD-7 and 20% w/w of **AH10** or **AH11** in 2 mL chlorobenzene was thoroughly mixed for 2 h at 50 °C; it was then filtered through a 0.45 µm pore filter and spin-coated at 2500 rpm for 1 min on top of the PEDOT:PSS layer and baked for 10 min at 120 °C to form the emissive layer of thickness 93 nm as measured by an ellipsometer. Each sample was shadow masked to produce four pixels with three different device areas, 4 × 4 mm, 2 × 2 mm and two 4 × 2 mm, as shown in Fig.4. The samples were then introduced into a nitrogen glove box, where 30 nm of 2,2′,2″-(1,3,5-benzenetriyl)tris(1-phenyl-1H-benzimidazole) (TPBi) was evaporated as an electron injection/hole-blocking layer at a rate of *ca* 1 A s^{-1} under vacuum at a pressure of *ca* 1 × 10^{-6} Torr, followed by 0.8 nm LiF and a 100 nm capping layer of aluminium under the same evaporation conditions. All samples were encapsulated in a glove box using DELO UV cured epoxy (KATIOBOND), capped with a 1.2 × 1.2 cm microscope glass slide, and then exposed to UV light for 4 min. Current–voltage data, device efficiency, brightness and electroluminescence spectra were measured in a calibrated Labsphere LMS-100 integrating sphere. A bespoke NI LabVIEW program was used to control an Agilent 6632B DC power supply, and the emission properties of the device were measured using an Ocean Optics USB4000 CCD fibre optic spectrometer.

RESULTS AND DISCUSSION

Although the synthesis of 5-(perylen-3-yl)pent-4-yn-1-ol had been previously reported[37,45] we found that a slight modification of this procedure afforded higher yields (66%) in a more reproducible manner. The PLA-perylene polymer(AH11) was synthesised using a simple protocol involving the ring opening polymerisation of L-LA with a suitable hydroxylated perylene derivative as an initiator in the presence of DBU as a catalyst at ambient temperature.[47] The use of DBU allows a high degree of polymerisation, very narrow molecular weight distributions and a low catalyst concentration of 1 mol%. This methodology is preferable to that employing stannous octanoate, one of the most commonly used catalysts currently employed for the promotion of these polymerisation reactions, and is experimentally easy to adopt.[48–50] Most notably, the DBU-catalysed process does not utilise toxic tin-based reagents which limits their potential utility, especially in the context of biomedical applications. The polymers generated in our study were fully characterised spectroscopically (IR, ^{1}H NMR and ^{13}C NMR) and using GPC. The molecular weight distributions of the **AH10** and **AH11** are listed in Table 1; these polymers have M_n values similar to those recently reported for polymers derived from the ring opening polymerisation of L-LA with pyrenebutanol.[48]

Figure 1(a) shows the ^{1}H NMR spectra of the polymers, highlighting the –CH and –CH_3 protons in poly-L-lactide. The resonance at δ 4.3 ppm corresponds to H_h derived from the terminal CH–OH residue, and that at δ 5.2 ppm corresponds to H_f in the polymer backbone. The resonances between 1.3 and 1.7 ppm are characteristic of the –CH_3 groups in the backbone of the polymer and the end group of the poly-L-lactide. The ^{13}C NMR spectrum of **AH11** is presented in Fig. 1(b). These data indicate the presence of the lactide carbonyl, methyl (–CH_3) and methine (–CH) groups at 168, 18 and 68 ppm, respectively; the remaining methylene resonances (–CH_2) appear between 30 and 72 ppm while the perylene carbons appear in the region typical of aromatic compounds (120–132 ppm). All of the polymers showed IR absorptions at 1746 cm^{-1} typical of that for a saturated ester carbonyl moiety, as shown in Fig. S2.

The thermal properties of the polylactides **AH10** and **AH11** were studied by TGA and DSC. The degradation behaviour of 5.6 mg samples of the polymer was measured under a nitrogen atmosphere when heated from 30 °C to 600 °C at a constant heating rate of 10 °C min^{-1}. The T_i, T_f, $T_{50\%}$ and char content (%) at 300 °C were determined and are compiled in Table S1 in Appendix S1. The rate of decomposition (%wt min^{-1}) was calculated from the slope of the degradation curve between 20% and 80% weight loss. Figure 2(b) shows that the decomposition process consists of one stage starting at 208 °C and 217 °C for **AH10** and **AH11** respectively. The char content for **AH10** and **AH11** was found to be 9.11 and 6.75 wt% respectively. The curve was almost constant when the temperature was below 180 °C, indicating that there was no degradation, and at 200 °C the degradation was only 9% for **AH11** and less than 6% for **AH10**. Both materials therefore have good thermal stability below 180 °C making them suitable candidates for device fabrication.[29,35]

The thermal transition temperatures of the prepared polymers were analysed from DSC thermograms as shown in Fig. 2(a) and

Polymer International published by John Wiley & Sons Ltd on behalf of Society of Industrial Chemistry.

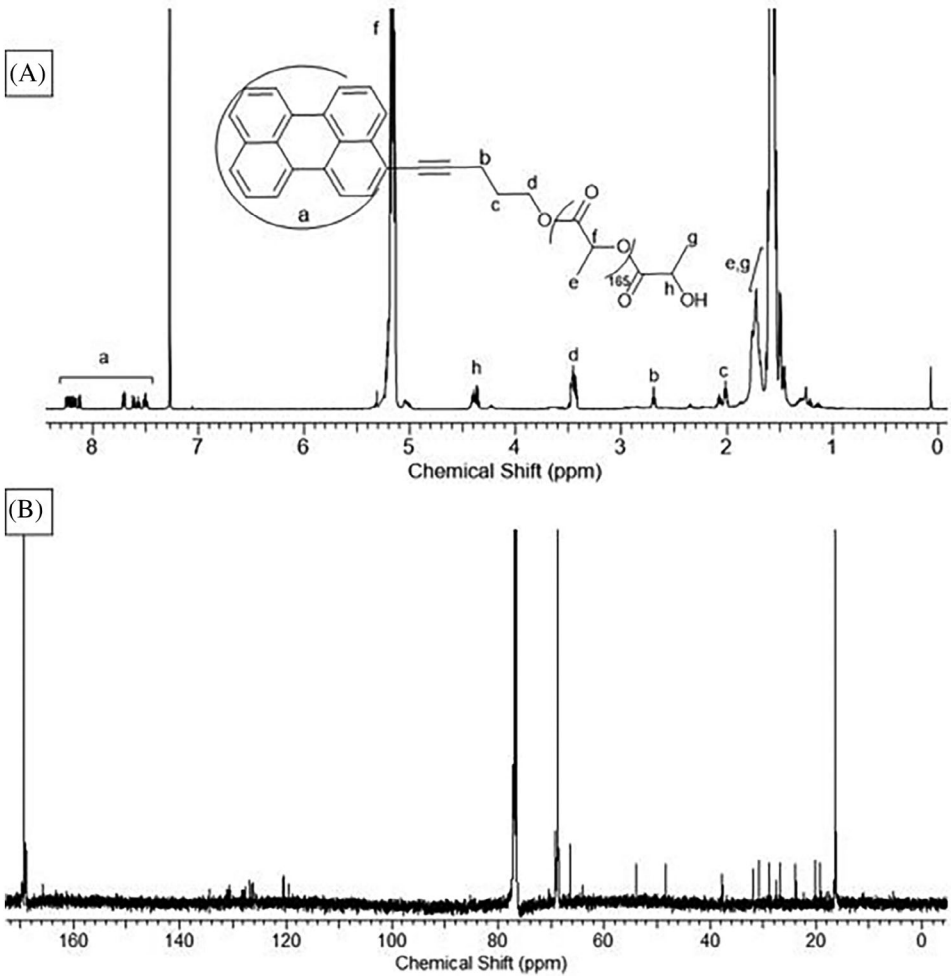

Figure 1 (A) ^{1}H NMR spectrum (500 MHz, $CDCl_3$) and (B) ^{13}C NMR spectrum (126 MHz, $CDCl_3$) of **AH11**.

Table S1 in Appendix S1. From the first heating scan, the glass transitions T_g of the prepared polymers were 56 °C and 45 °C for **AH10** and **AH11** respectively, while the crystallisation temperatures T_c were 129 °C and 102 °C for **AH10** and **AH11** respectively (Table S2). There were two endothermal peaks corresponding to the crystallisation temperatures for perylene polymer **AH11**. Apparently, there is not enough time for the amorphous PLA chain to adjust well on increasing the heating rate.[36]

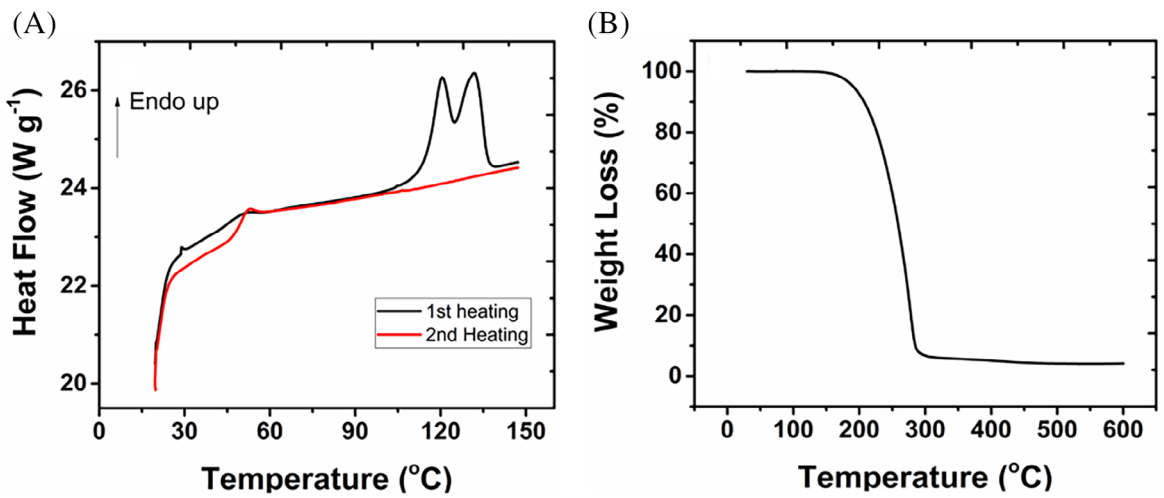

Figure 2 (A) DSC thermograms of **AH11**. (B) TGA thermograms of **AH11**.

Table 1 Molecular weight distributions for **AH10**[44] and **AH11**

Polymer	M_w/M_n[a] (Da)	M_n (Da)[b]	ĐM
AH10	5500/3200	4600	1.72
AH11	12 511/5853	12 485	2.13

ĐM is the ratio of the weight-average molecular weight M_w to the number-average molecular weight M_n.
[a]Determined by GPC analysis.
[b]Determined by ^{1}H NMR (Fig. 1(A) .

Materials photophysics

The normalised UV–visible spectrum of **AH10** in CH_2Cl_2 (0.6 mg mL^{-1}) shows absorption bands at 345 nm that can be assigned to $S_0 \rightarrow S_2$ transitions in the pyrene nucleus; a low intensity, higher energy transition, $S_0 \rightarrow S_1$, at 375 nm is also apparent[37] (Fig. 3(a)). In comparison to **AH10**, the UV–visible spectrum for **AH11** has absorption bands at 381, 405, 428 and 457 nm (Fig. 3(b)). The fluorescence spectra of **AH10** and **AH11** were measured with λ_{ex} at the $S_0 \rightarrow S_2$ transition, *ca* 340 nm for pyrene lactide polymer and at 420 nm for perylene lactide polymer at concentrations of 0.06 mg mL^{-1} in CH_2Cl_2. The pyrene polymer shows four emission signals at 375, 379, 416 and 440 nm. Similarly, the perylene polymer **AH11** also exhibits four emission signals at 466, 498, 530 and 576 nm whose values were concentration independent. These spectra were also largely devoid of any longer wavelength emissions, which are characteristic of excimer emissions for aggregated structures; this indicates that the polycyclic aromatic hydrocarbon units are essentially isolated.

OLED device characteristics

Since the pyrene emission is in the deep blue–UV region, the OLED devices prepared in this study using **AH10** show very weak emission mainly due to exciton quenching by the low triplet energy levels. Given that our device characterisation system is suitable for measuring accurately visible light between 400 and

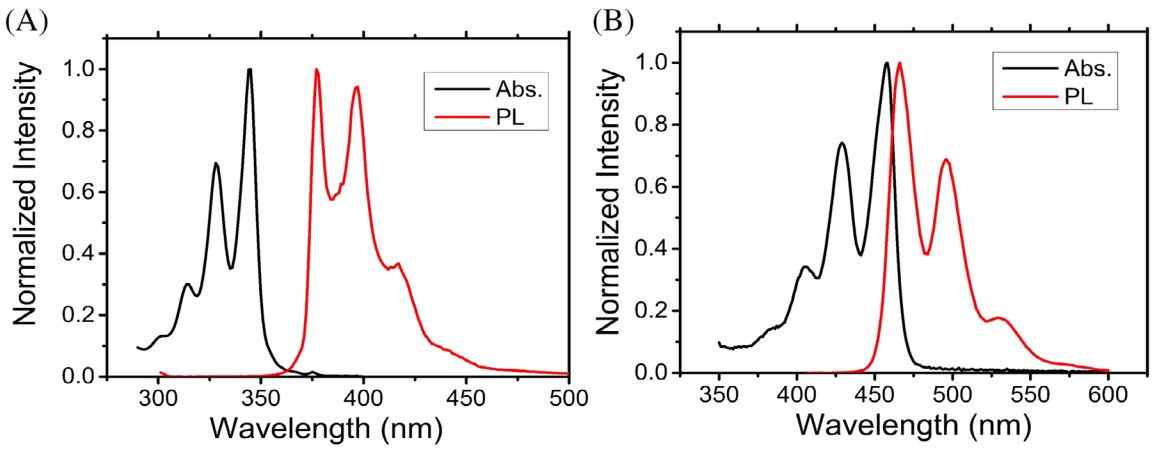

Figure 3 Normalised UV–visible absorption and fluorescence spectra of **AH10** (λ_{ex} = 340 nm) (A) and **AH11** (λ_{ex} = 420 nm) (B).

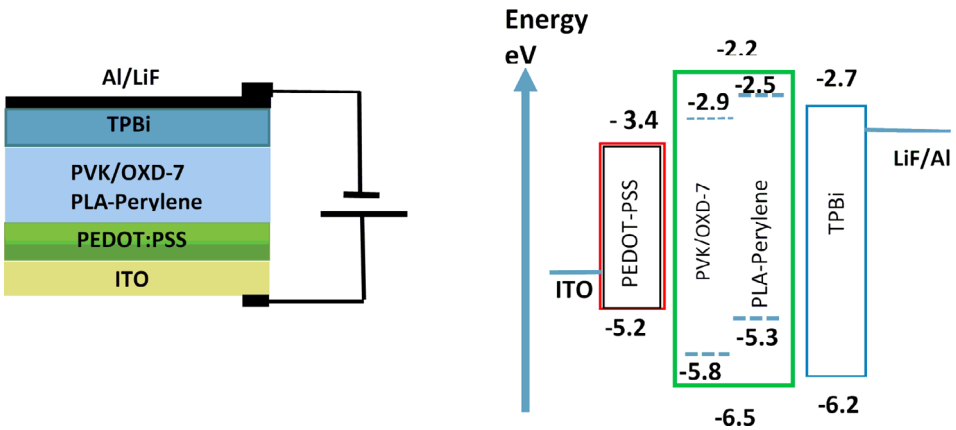

Scheme 1 The device architecture and energy levels for materials used in the device.

700 nm and is not calibrated to correctly measure the UV region of light <400 nm, only OLED devices that used **AH11** are fully characterised; they exhibit a reasonable device performance. A deep blue <400 nm electroluminescence emission from **AH10** was not characterised due to the lack of system sensitivity at UV wavelengths.

The device architecture and the schematic energy level diagrams for materials used in the device are shown in Scheme 1.

The highest occupied molecular orbital (HOMO) and lowest unoccupied molecular orbital (LUMO) energy levels for perylene are −5.3 eV and −2.5 eV respectively.[51] In a single emissive layer device consisting of PVK, OXD-7 and **AH11**, the injected electrons from the aluminium (Al) cathode (−4.2 eV) modified by LiF provide easy injection to the TPBi layer. The LUMO energy level of OXD-7 is located at −2.9 eV which is only 0.2 eV higher than the LUMO of TPBi (−2.7 eV); therefore most of the injected electrons in the TPBi layer are captured and transported by the OXD-7. Since the perylene LUMO energy level resides at −2.5 eV, some of the OXD-7 electrons are trapped in the perylene LUMO. In passing we note that, in an initial analysis, replacement of the perylene fluorophore by pyrene results in less efficient electrons because the LUMO energy level of pyrene at −2.3 eV is 0.6 eV higher than the OXD-7 LUMO, an effect that we are currently exploring.. At the anode side, the nearest HOMO energy level to the PEDOT:PSS at −5.2 eV is the HOMO level of PVK at −5.8 eV. However, direct injection of the holes from PEDOT:PSS to the perylene HOMO energy levels at −5.3 eV is also possible, but with the low concentration content of perylene we expect that the hole trapping in the HOMO energy level of the perylene mainly comes from the hole transport of the PVK. Similar hole trapping efficiency occurs in the pyrene HOMO energy level at −5.67 eV which closely matches the HOMO energy level of the PVK at −5.8 eV. The relative HOMO–LUMO energy levels of various materials are not the only factor affecting device efficiency. Charge balance and the effect of the triplet energy quenching are also factors that control exciton formation and concentration. Charge balance can be controlled by adjusting the PVK:OXD-7 concentration ratio in addition to the TPBi thickness. Charge balance optimisation was studied by varying the OXD-7 concentration within the PVK. The best OXD-7 concentration was found at 35%–40% w:w with respect to PVK. The final important factor affecting the device efficiency is the triplet energy levels of the PVK and OXD-7 with respect to those of the perylene or pyrene triplet state. The triplet energy level

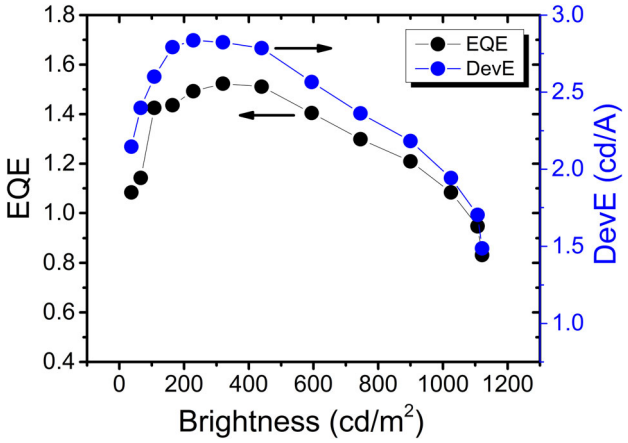

Figure 5 Device efficiencies at different brightnesses for the device structure ITO/PEDOT/PVK:OXD-7:**AH11**/TPBi/LiF:Al.

for OXD-7 is 2.7 eV and that for PVK is 2.88 eV (monomer) and 2.46 eV (dimer). For the generated excitons in the pyrene or perylene their triplet energy levels should be lower than that for OXD-7 and PVK. Since the triplet energy level of perylene is higher than OXD-7 and PVK, Dexter energy transfer may occur from the triplet excitons on the perylene or pyrene to the low-lying triplet states of PVK and OXD-7. This will bleach the triplet energy states and increase the intersystem crossing from the perylene or pyrene singlet to their triplet which reduces the fluorescence quantum yields.

Figure 4 shows the brightness of the OLED device using **AH11** as the emissive material. The turn-on voltage at 10 cd m^{-2} is about 6 V and the maximum brightness reaches 1200 cd m^{-2} at 13 V. The corresponding external quantum efficiency and device current efficiency are 1.5% and 2.8 cd A^{-1} respectively (Fig. 5**)**. The electroluminescence spectrum (Fig. 6**)** has the same profile as the photoluminescence spectrum in a dilute solution (Fig. 3**)**. This confirms that perylene molecules are isolated on the PLA backbone with no ground state complex formation or π–π stacking, which leads to strong intermolecular interactions in the solid state and a substantial red shift of their fluorescence emission. We believe that the 8 nm red shift observed in the electroluminescence spectrum compared with the photoluminescence spectrum is due to differences in the spectrometer calibration. A

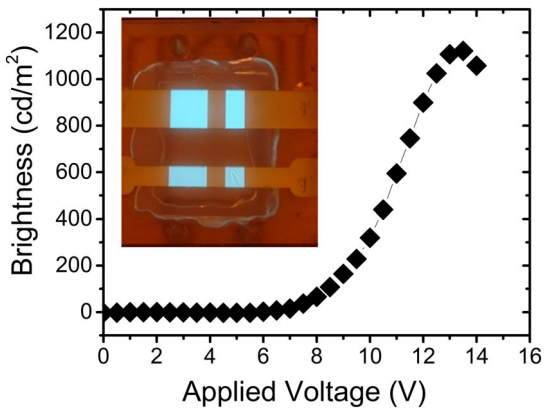

Figure 4 Device brightness as a function of applied voltage; the inset is a photograph of the four devices (pixels) in one sample of the device structure ITO/PEDOT/PVK:OXD-7:**AH11**/TPBi/LiF:Al.

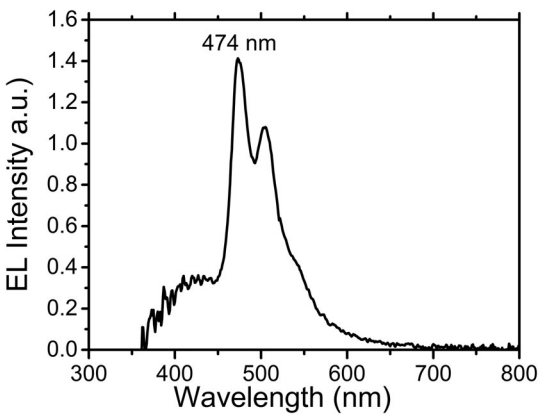

Figure 6 Device electroluminescence emission profile for the device structure ITO/PEDOT/PVK:OXD-7:**AH11**/TPBi/LiF:Al.

broad shoulder at 420 nm may be a consequence of the emission from the PVK which normally appears in the case of incomplete energy transfer from the PVK to the perylene, due to weak spectral overlap between the PVK emission with the perylene absorption which prevents sufficient Förster energy transfer.[51]

CONCLUSION

In this work we have demonstrated, for the first time, the feasibility of using biocompatible and biodegradable PLA as a matrix for the active emitting layer of an OLED device. The device efficiency can be increased further if the electron and hole transport materials are also attached to the PLA backbones. The major drawback to the present construct is the low pyrene and perylene concentration within the PLA matrix; hence increasing the pyrene and perylene concentration within the PLA matrix will reduce the resistivity property of the PLA and increase the dopant sites to generate more emissive excitons. Our study also shows that the use of PVK and OXD-7 does not lead to optimal charge balance because phase segregation in the solution processed OLED device leads to an increase in the device dark current and reduces the efficiency. We posit that incorporation of additional high triplet electron and transport materials into the backbone of the PLA will result in enhanced performance of these materials. We envisage that downstream applications of this initial study could lead to the development of new photodynamic therapy treatments,[52,53] an outcome which is prescient due to the modular nature and tunability of the fluorophore synthesis. Work in this area is currently under investigation.

ACKNOWLEDGEMENT

A. A. Alwattar gratefully acknowledges the Iraqi Ministry of Higher Education and Scientific Research (MOHER) and the University of Basrah (Chemistry Department) for the provision of a research scholarship. The University of Manchester thanks the EPSRC for the provision of Bruker NMR spectrometers (EP/K039547/1).

SUPPORTING INFORMATION

Supporting information may be found in the online version of this article.

REFERENCES

1 Berggren M and Richter-Dahlfors A, *Adv Mater* **19**:3201–3213 (2007). https://doi.org/10.1002/adma.200700419.
2 Yambem SD, Brooks-Richards TL, Forrestal DP, Kielar M, Sah P, Pandey AK *et al.*, *Sci Rep* **9**:9875 (2019). https://doi.org/10.1038/s41598-019-45867-9.
3 Mühl S and Beyer B, *Electronics* **3**:444–461 (2014). https://doi.org/10.3390/electronics3030444.
4 Irimia-Vladu M, *Chem Soc Rev* **21**:588–610 (2014). https://doi.org/10.1039/c3cs60235d.
5 Mattana G, Briand D, Marette A, Vásquez Quintero A and De Rooij NF, *Org Electron* **17**:77–86 (2015). https://doi.org/10.1016/j.orgel.2014.11.010.
6 Hwang S-W, Song J-K, Huang X, Cheng H, Kang S-K, Kim BH *et al.*, *Adv Mater* **26**:3905–3911 (2014). https://doi.org/10.1002/adma.201306050.
7 Yoo S, Kim YH, Ka JW, Kim YS, Yi MH and Jang KS, *Org Electron* **23**:213–218 (2015). https://doi.org/10.1016/j.orgel.2015.05.012.
8 Jin SH, Kang S-K, Cho I-T, Han SY, Chung HU, Lee DJ *et al.*, *ACS Appl Mater Interfaces* **7**:8268–8274 (2015). https://doi.org/10.1021/acsami.5b00086.
9 Eder F, Klauk H, Halik M, Zschieschang U, Schmid G and Dehm C, *Appl Phys Lett* **84**:2673–2675 (2004). https://doi.org/10.1063/1.1690870.
10 Hübler A, Trnovec B, Zillger T, Ali M, Wetzold N, Mingebach M *et al.*, *Adv Energy Mater* **1**:1018–1022 (2011). https://doi.org/10.1002/aenm.201100394.
11 Zschieschang U, Yamamoto T, Takimiya K, Kuwabara H, Ikeda M, Sekitani T *et al.*, *Adv Mater* **23**:559–559 (2011). https://doi.org/10.1002/adma.201190006.
12 Shafiee H, Asghar W, Inci F, Yuksekkaya M, Jahangir M, Zhang MH *et al.*, *Sci Rep* **5**:1–9 (2015). https://doi.org/10.1038/srep08719.
13 Tao H, Brenckle MA, Yang M, Zhang J, Liu M, Siebert SM *et al.*, *Adv Mater* **24**:1067–1072 (2012). https://doi.org/10.1002/adma.201103814.
14 Wang C-H, Hsieh C-Y and Hwang J-C, *Adv Mater* **23**:1630–1634 (2011). https://doi.org/10.1002/adma.201004071.
15 Irimia-Vladu M, Troshin PA, Reisinger M, Schwabegger G, Ullah M, Schwoediauer R *et al.*, *Org Electron* **11**:1974–1990 (2010). https://doi.org/10.1016/j.orgel.2010.09.007.
16 Acar H, Çınar S, Thunga M, Kessler MR, Hashemi N and Montazami R, *Adv Funct Mater* **24**:4135–4143 (2014). https://doi.org/10.1002/adfm.201304186.
17 He Y, Sun J, Qian C, Kong L a, Jiang J, Yang J *et al.*, *Org Electron* **38**:357–361 (2016). https://doi.org/10.1016/j.orgel.2016.09.017.
18 Irimia-Vladu M, Sariciftci NS and Bauer S, *J Mater Chem* **21**:1350–1361 (2011). https://doi.org/10.1039/c0jm02444a.
19 Zhu H, Luo W, Ciesielski PN, Fang Z, Zhu JY, Henriksson G *et al.*, *Chem Rev* **24**:9305–9374 (2016). https://doi.org/10.1021/acs.chemrev.6b00225.
20 Yuen JD, Walper SA, Melde BJ, Daniele MA and Stenger DA, *Sci Rep* **7**:1–9 (2017). https://doi.org/10.1038/srep40867.
21 Li R, Wang L, Kong D and Yin L, *Bioact Mater* **3**:322–333 (2018). https://doi.org/10.1016/j.bioactmat.2017.12.001.
22 Liu X, Shi M, Luo Y, Zhou L, Loh ZR, Oon ZJ *et al.*, *Appl Sci* **10**:1320–1347 (2020). https://doi.org/10.3390/app10041320.
23 Zhang Y, Zhang Q, Zha L, Yang W, Wang C, Jiang X *et al.*, *Colloid Polym Sci* **282**:1323–1328 (2004). https://doi.org/10.1007/s00396-004-1068-5.
24 Ray SS, Yamada K, Okamoto M and Ueda K, *Macromol Mater Eng* **288**:203–208 (2003). https://doi.org/10.1002/mame.200390013.
25 Madhavan Nampoothiri K, Nair NR and John RP, *Bioresour Technol* **101**:8493–8501 (2010). https://doi.org/10.1016/j.biortech.2010.05.092.
26 Guo R, Ren Z, Bi H, Xu M and Cai L, *Polymers* **11**:549–557 (2019). https://doi.org/10.3390/polym11030549.
27 Nakagawa T, Nakiri T, Hosoya R and Tajitsu Y, *IEEE Trans Ind Appl* **40**:1020–1024 (2004). https://doi.org/10.1109/TIA.2004.830751.
28 Chu Y, Wu X, Lu J, Liu D, Du J, Zhang G *et al.*, *Adv Sci* **3**:1500435–1500440 (2016). https://doi.org/10.1002/advs.201500435.
29 Wu X, Chu Y, Liu R, Katz HE and Huang J, *Adv Sci* **4**:1700442–1700452 (2017). https://doi.org/10.1002/advs.201700442.
30 Zimmermann J, Jürgensen N, Morfa AJ, Wang B, Tekoglu S and Hernandez-Sosa G, *ACS Sustainable Chem Eng* **4**:7050–7055 (2016). https://doi.org/10.1021/acssuschemeng.6b01953.
31 Gao M, Shih CC, Pan SY, Chueh CC and Chen WC, *J Mater Chem A* **30**:20546–20563 (2018). https://doi.org/10.1039/C8TA07246A.
32 La Mattina AA, Mariani S and Barillaro G, *Adv Sci* **7**:1902872–1902905 (2020). https://doi.org/10.1002/advs.201902872.
33 Lu D, Liu T, Chang J, Peng D, Zhang Y, Shin J *et al.*, *Adv Mater* **31**:1902739 (2019). https://doi.org/10.1002/adma.201902739.
34 Jürgensen N, Ackermann M, Marszalek T, Zimmermann J, Morfa AJ, Pisula W *et al.*, *ACS Sustainable Chem Eng* **5**:5368–5372 (2017). https://doi.org/10.1021/acssuschemeng.7b00675.
35 Zhu H, Xiao Z, Liu D, Li Y, Weadock NJ, Fang Z *et al.*, *Energy Environ Sci* **6**:2105–2111 (2013). https://doi.org/10.1039/c3ee40492g.
36 Mucur S, Pi II, Tumay TAI, Birdoğan S, San SE and Tekin E, *Nano-Struct Nano-Objects* **1**:7–14 (2015). https://doi.org/10.1016/j.nanoso.2015.01.001.
37 Barrett ES, Dale TJ and Rebek J. Synthesis and assembly of monofunctionalized pyrogallolarene capsulesmonitored by fluorescence resonance energy transfer. *Chem Commun* 4224–4226 (2007).
38 Li J, Yang C, Peng X, Chen Y, Qi Q, Luo X *et al.*, *J Mater Chem C* **6**:19–28 (2017). https://doi.org/10.1039/c7tc03780e.
39 Li J, Hou C, Huang C, Xu S, Peng X, Qi Q *et al.*, *Research* **2020**:3839160 (2020). https://doi.org/10.34133/2020/3839160.
40 Zhang Q, Li B, Huang S, Nomura H, Tanaka H and Adachi C, *Nat Photonics* **8**:326–332 (2014). https://doi.org/10.1038/nphoton.2014.12.

41 Kim Y-H, Wolf C, Cho H, Jeong S-H and Lee T-W, *Adv Mater* **28**:734–741 (2016). https://doi.org/10.1002/adma.201504490.
42 Huang T, Jiang W and Duan L, *J Mater Chem C* **31**:5577–5596 (2018). https://doi.org/10.1039/c8tc01139g.
43 He Z, Wang C, Zhao J, Du X, Yang H, Zhong P *et al.*, *J Mater Chem C* **7**: 11806–11812 (2019). https://doi.org/10.1039/c9tc03468d.
44 Alwattar A, Haddad A, Zhou Q, Nascimento T, Greenhalgh R, Medeiros E *et al.*, *Polym Int* **68**:360–368 (2019). https://doi.org/10.1002/pi.5712.
45 Fan C, Wu W, Chruma JJ, Zhao J and Yang C, *J Am Chem Soc* **138**: 15405–15412 (2016). https://doi.org/10.1021/jacs.6b07946.
46 Torres É, Berberan-Santos MN and Brites MJ, *Dye Pigm* **112**:298–304 (2015). https://doi.org/10.1016/j.dyepig.2014.07.019.
47 Sherck NJ, Kim HC and Won Y-Y, *Macromolecules* **49**:4699–4713 (2016). https://doi.org/10.1021/acs.macromol.6b00621.
48 Farhangi S and Duhamel J, *Macromolecules* **49**:353–361 (2016). https://doi.org/10.1021/acs.macromol.5b02476.
49 Leng X, Wei Z, Ren Y, Li Y, Wang Y and Wang Q, *RSC Adv* **5**:81482–81491 (2015). https://doi.org/10.1039/c5ra15141d.
50 Wu GP, Darensbourg DJ and Lu XB, *J Am Chem Soc* **134**:17739–17745 (2012). https://doi.org/10.1021/ja307976c.
51 Chidirala S, Ulla H, Valaboju A, Kiran MR, Mohanty ME, Satyanarayan MN *et al.*, *J Org Chem* **81**:603–614 (2016). https://doi.org/10.1021/acs.joc.5b02423.
52 Bansal A, Yang F, Xi T, Zhang Y and Ho JS, *Proc Natl Acad Sci U S A* **115**:1469–1474 (2018). https://doi.org/10.1073/pnas.1717552115.
53 Lian C, Piksa M, Yoshida K, Persheyev S, Pawlik KJ, Matczyszyn K *et al.*, *NPJ Flex Electron* **3**:1–6 (2019). https://doi.org/10.1038/s41528-019-0058-0.